

不同温度锻造的 $\text{Ti}_2\text{AlNb}/\text{TC11}$ 双合金焊接 界面组织在热暴露时的变化

贾 倩^{1,2}, 姚泽坤^{1,2}, 张东亚^{1,2}, 秦 春^{1,2},
涂唯坚^{1,2}, 杨国宝^{1,2}, 耿景东³

(1. 西北工业大学 材料学院, 西安 710072; 2. 难变形材料锻造技术研究应用中心, 西安 710072;
3. 贵州航空动力公司 叶片分厂, 平坝 561114)

摘 要: 利用光学显微镜 OM 和 透射电子显微镜 TEM 研究了 $\text{Ti}_2\text{AlNb}/\text{TC11}$ 双合金经近等温锻造、梯度热处理后以不同时间在 550 °C 热暴露的显微组织变化。结果表明, 热暴露期间, 接头及 Ti_2AlNb 基体组织有 $\text{B2} \rightarrow \text{O} + \beta$ 分解发生, α_2 相向 B2 晶界迁移, 热暴露时间越长, α_2 相偏聚越严重, 在热暴露 100 h 时聚集成块状, 同时随热暴露时间的延长, β 相变得粗大, 体积分数增加, 当接头部位的铝、铌含量较高时, α_2 相在晶界偏聚成块, 同时原始 O 相与 B2 相分解而来的次生 O 相叠加而导致其粗化。

关键词: 双合金; 近等温锻造; 热暴露; 组织

中图分类号: TG 113.12 **文献标识码:** A **文章编号:** 0253-360X(2014)11-0079-05

0 序 言

航空发动机的核心部件, 如压气机盘、涡轮盘, 服役条件极其恶劣, 其盘缘和盘心的温差达到 200 ~ 300 °C; 盘缘、盘芯各部位承受的应力也大不相同^[1], 盘心部位承受应力大并要求具有高强度、高塑性和优良的低周疲劳性能; 而盘缘部位承受温度高, 要求具有优良的高温强度、蠕变抗力、裂纹扩展抗力及高的断裂韧性。上述盘件服役性能要求是单一材料、单一组织无法满足的, 因此双合金盘应运而生^[2]。当前最有前途的技术之一是采用质量较轻、力学性能与镍基高温合金相近的 Ti_3Al 、 Ti_2AlNb 等金属间化合物与中低温性能好的钛合金通过接合 + 等温成形技术, 制成双合金盘代替镍基高温合金做高压压气机盘^[3-6]。但异种合金结合界面受结合方式、元素扩散引起的化学成分变化的影响, 常导致界面组织变化而影响接头处的性能^[7-9]。文中通过光学显微镜和透射电子显微镜观察不同热暴露时间下真空电子束焊接加近等温锻造的 $\text{Ti}_2\text{AlNb}/\text{TC11}$ 双合金界面组织, 探索焊接界面在长期高温热负荷作用下组织的变化规律, 为双合金盘应用提供理论依据。

1 试验方法

试验所用的 Ti_2AlNb 合金是北京钢铁研究总院提供的锻态方料, 其名义成分为: $\text{Ti}-22\text{Al}-25\text{Nb}$ (原子分数, %)。金相法测定该合金的相变点为 1 045 °C。TC11 合金是宝鸡有色金属加工厂提供的轧制态棒材, 其成分为 (质量分数, %): 6.5% Al, 3.5% Mo, 2.0% Zr, 0.25% Si, 其余为钛。该合金的相变点为 995 °C。

1.1 原材料改锻和焊接

两种合金均在空气锤上改锻。 Ti_2AlNb 合金始锻温度为 1 040 °C, 终锻温度大于 950 °C, 保温时间为 1 h。TC11 合金始锻温度为 960 °C, 终锻温度大于 880 °C, 保温时间为 0.5 h。锻后空冷。改锻的两种合金分别切成 25 mm × 25 mm × 35 mm 的条块, 并将待焊接面磨平, 用丙酮清洗干净。在德国 IGM 公司制造的 EBCAM KS55-G150-CNC 型真空电子束焊机上进行焊接。焊接电压为 150 kV, 聚焦电流为 2 170 mA, 焊接电流为 28 mA, 焊接速度为 8 mm/s。

1.2 近等温锻造及热处理和热暴露试验

近等温锻造温度为 1 025 °C 和 995 °C, 变形 40%, 应变速率为 $10^{-2} \cdot \text{s}^{-1}$, 试样沿轴向进行侧压, 试样表面涂 FR21 玻璃润滑剂。试样锻后先经 960 °C, 1.5 h, AC (air cool) 的固溶处理, 接着进行梯度时效处理, 即: 800 °C ($\text{Ti}-22\text{Al}-25\text{Nb}$ 侧) / 530 °C

(TC11 侧), 6 h, AC 取样在光镜(OM)及透射电子显微镜(TEM)上进行组织形貌观察.

热处理后的试样分别进行 50 h 和 100 h 热暴露试验, 热暴露温度均为 $550\text{ }^{\circ}\text{C} \pm 3\text{ }^{\circ}\text{C}$, 截取焊缝区观察不同时间热暴露后的显微组织变化.

2 试验结果与分析

温度 $1\ 025\text{ }^{\circ}\text{C}$ 近等温锻造和热处理的 Ti_2AlNb /TC11 异种合金接头试样在焊缝中心与两侧基体的显微组织如图 1~图 4 所示.

图 1a 为热暴露前 TC11 侧的显微组织. 由于变形开始温度高于 TC11 的相变点, 同时变形较大, 原

始 β 晶界已被破碎, 形成等轴状的 α 相. 随着变形的进行, 温度下降, 从原始 β 晶内析出条片状 α 相, 其后热处理固溶时, 条片状 α 相大部分保留下来, 与再结晶球状 α 相一起形成双态组织. 比较图 2a 可以看出, 热暴露 50 h 后, 从 $\beta_{\text{转}}$ 中析出了次生针状 α 相, 当热暴露时间延长至 100 h, 片状 α 相数量减少 (图 3a). 这是由于热暴露时间的延长, Ti 元素从 TC11 侧不断向焊区扩散, 使得原来的 α 条发生部分溶解, 原子排列层减薄. 板条间片间距增加所致. 图 1b 为热暴露前焊缝中心的显微组织, 焊缝区内的晶界由断续可见的条状和等轴状 O/α_2 相构成, 晶内 O/α_2 相多为棒状和球状, 只有少量条状, 同时还有少量等轴状 β 相, 通常 α_2 相在 O 相边缘生成, 并在

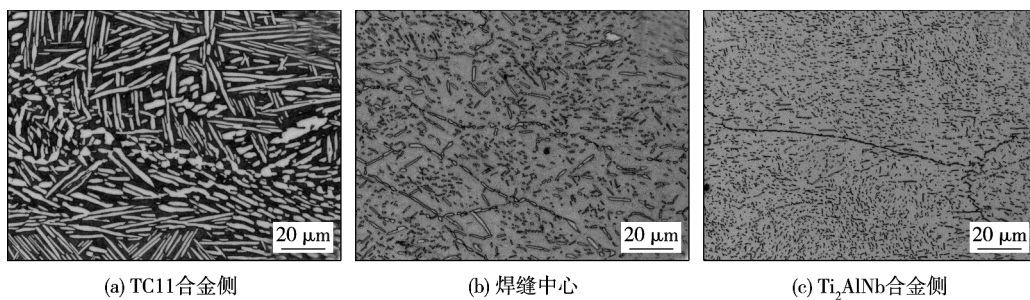


图 1 $1\ 025\text{ }^{\circ}\text{C}$ 锻造及热处理后的 Ti_2AlNb /TC11 界面组织

Fig. 1 Microstructures of Ti_2AlNb /TC11 joint forged at $1\ 025\text{ }^{\circ}\text{C}$ and heat treatment

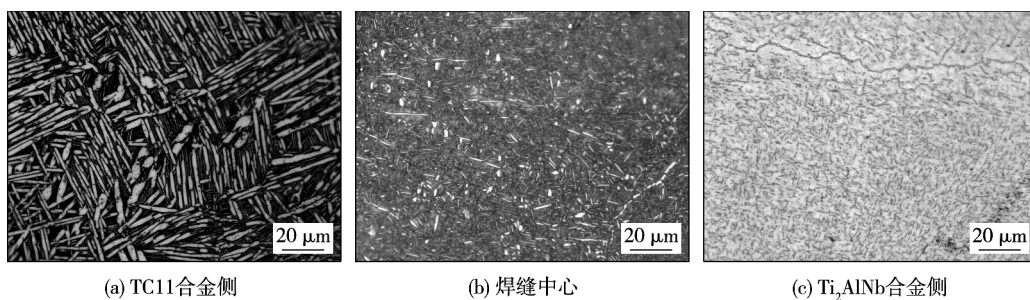


图 2 $1\ 025\text{ }^{\circ}\text{C}$ 锻造及热处理后的 Ti_2AlNb /TC11 焊接界面经 50 h 热暴露后的组织

Fig. 2 Microstructures of Ti_2AlNb /TC11 joint forged at $1\ 025\text{ }^{\circ}\text{C}$ and heat treatment after thermal exposure for 50 h

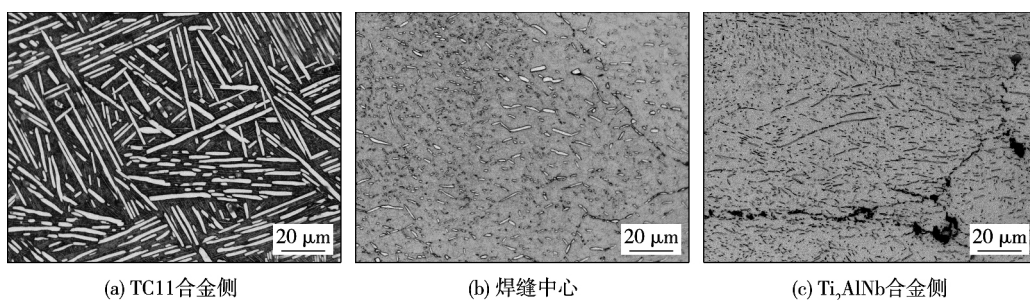
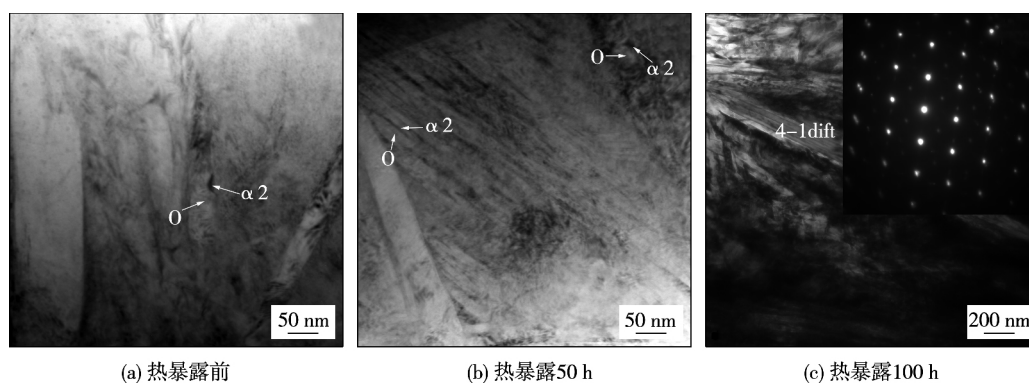


图 3 $1\ 025\text{ }^{\circ}\text{C}$ 锻造及热处理后的 Ti_2AlNb /TC11 焊接界面经 100 h 热暴露后的组织

Fig. 3 Microstructures of interface of Ti_2AlNb /TC11 joint forged at $1\ 025\text{ }^{\circ}\text{C}$ and heat treatment after thermal exposure for 100 h

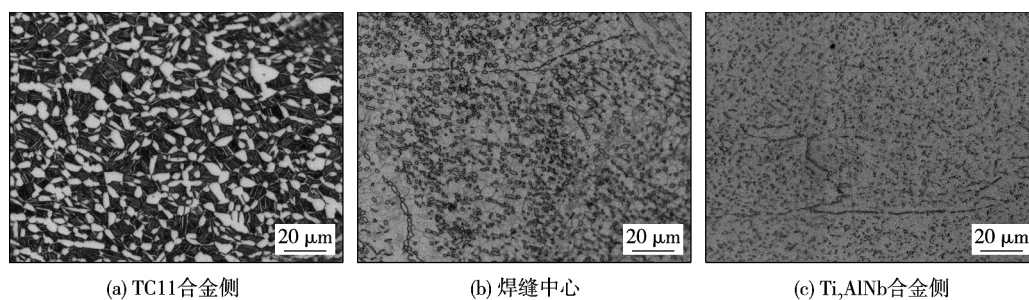
图 4 1 025 °C 锻造试样经热暴露不同时间的 $\text{Ti}_2\text{AlNb}/\text{TC11}$ 双合金界面透射Fig. 4 TEM image of $\text{Ti}_2\text{AlNb}/\text{TC11}$ dual alloy weld seam with different thermal exposure time forging at 1025 °C

热处理时保存下来(图 4a). 晶界呈断续状分布是由于变形较大, 晶界处积累位错多的地方发生了再结晶, 致使连续晶界破碎; 又因 B2 相晶粒内部的 α_2 相为硬质相, 因此, 硬相在变形软相的拉伸作用下, 会发生位错穿过硬相使其断开^[10]. 晶内尺寸较大的条状、棒状和等轴状相是固溶期间形成的, 尺寸较小的等轴状相是时效期间从 B2 基体中分解成的次生相. 热暴露 50 h 后(图 2b), β 相数量增加, 既有条状也有球状, 次生条状相数量也有增加, 但同时也发生了部分球化(图 4b), 这是长时间的高温热暴露导致介稳 B2 相发生 $\text{B2} \rightarrow \beta + \text{O}$ 的分解所致, 这时多余的 Al, Nb 元素扩散, 造成相晶格重建, 最终转化成 α_2 相. 随着热暴露时间延长至 100 h(图 3b), β 相数量增加, 尺寸增大, 同时 α_2 相向晶界迁移, 并在

B2 晶界处有间断的聚集, 这是 Al, Nb 元素从 Ti_2AlNb 侧不断向 TC11 侧扩散, 导致焊缝处这两种元素含量增加, 引起 α_2 相数量增加, 并在 B2 晶界逐渐聚集成块, 如图 4c 衍射图像所证明.

从图 1c 为 Ti_2AlNb 侧的显微组织中可以看出, 细小的条状及针状的 α_2 相、O 相均匀分布于 B2 基体中, 且 α_2 相数量较多, 尤其在晶界上. 热暴露 50 h 后(图 2c), α_2 相数量减少, 尺寸增大, O 相数量略有增加, 晶界上原来呈条状的 α_2 相已为 O 相断开而球化, 其厚度增加, 这仍然是元素扩散, 聚集长大所致. 随着热暴露时间延长至 100 h(图 3c), α_2 相在晶界上聚集成块.

995 °C 近等温锻造和热处理试样热暴露前后的焊缝中心与两侧基体的显微组织见图 5 ~ 图 8.

图 5 995 °C 锻造及热处理后的 $\text{Ti}_2\text{AlNb}/\text{TC11}$ 界面组织Fig. 5 Microstructures of $\text{Ti}_2\text{AlNb}/\text{TC11}$ joint forged at 995 °C and heat treatment

由图 5a ~ 图 7a 可以看出, 锻造温度为 995 °C 时, TC11 合金侧为双态组织即等轴 α 相及其间分布细条状 $\beta_{\text{转}}$ 相, 热暴露后, 只有 $\beta_{\text{转}}$ 中细小 α 条有所细化. 图 5b ~ 图 7b 为结合界面组织, 未热暴露时, B2 基体晶界由断续的条状 O 相及球状 O/ α_2 相构成, 这从图 8a 所示可以看出, 因 α_2 相偏聚于 B2 相边界上, 隔断了组成 B2 晶界的 O 相, 从光学图片中就看到条状和球状断续相连的 B2 晶界(图 5b). 晶

内基本为球状 O/ α_2 相, 热暴露 50 h 后, 条状 O 相一部分消失, 一部分粗化, 是由于热暴露期间发生了 $\text{B2} \rightarrow \beta + \text{O}$ 的分解, 但 β 条很细很窄(图 8b), 造成原 B2 晶界的 O 相与分解出的 O 相相连, 光学照片上就显示出等轴 O 相有所长大. 热暴露 100 h 后, B2 晶界上 O 相已完全球化, 就像珍珠项链一样相连, 粒状 α_2 相数量有所增加, 从透射电镜衍射图像图 8c 可以看到 β 相存在且随热暴露时间延长而迁

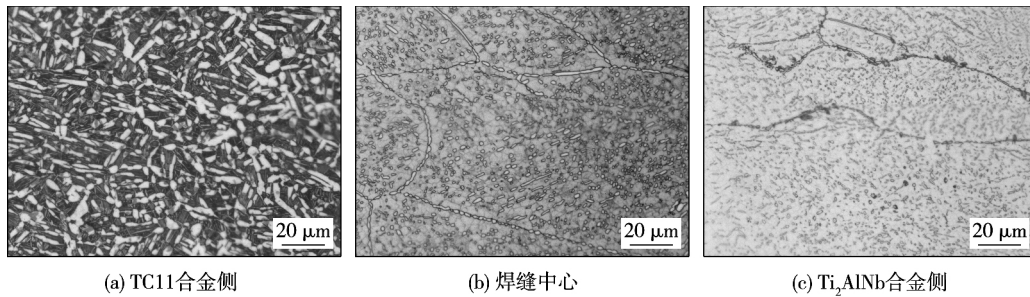


图 6 995 °C 锻造并热处理的 $\text{Ti}_2\text{AlNb}/\text{TC11}$ 焊接界面经 50 h 热暴露后的组织

Fig. 6 Microstructures of $\text{Ti}_2\text{AlNb}/\text{TC11}$ joint forged at 995 °C and heat treatment after thermal exposure for 50h

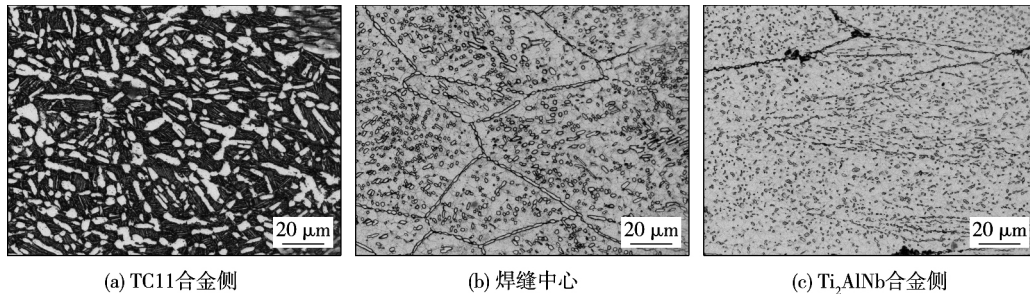


图 7 995 °C 锻造及热处理的 $\text{Ti}_2\text{AlNb}/\text{TC11}$ 焊接界面经 100 h 热暴露后的组织

Fig. 7 Microstructures of interface at $\text{Ti}_2\text{AlNb}/\text{TC11}$ joint forged at 995 °C and heat treatment after thermal exposure for 100 h

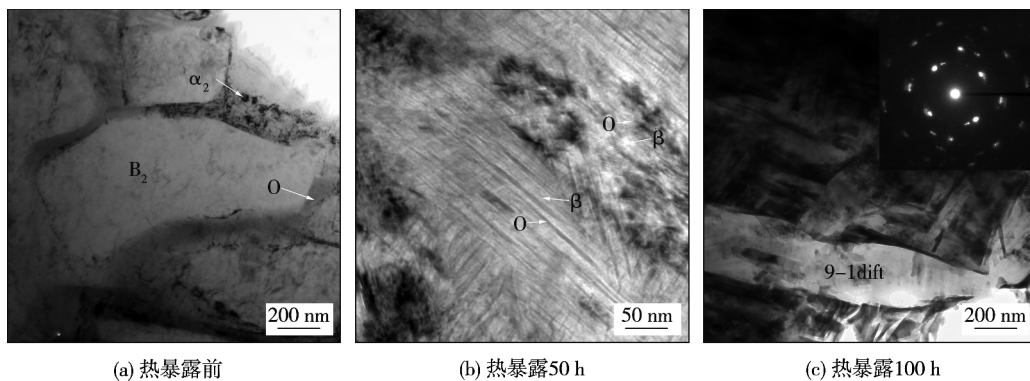


图 8 锻造温度为 995 °C 时不同热暴露时间的 $\text{Ti}_2\text{AlNb}/\text{TC11}$ 双合金界面透射图像

Fig. 8 TEM image of $\text{Ti}_2\text{AlNb}/\text{TC11}$ dual alloy welding seam with different thermal exposure time forging at 995 °C

移、合并长大. Ti_2AlNb 侧最大的变化是热暴露后 α_2 相在晶界聚集, 热暴露时间越长, α_2 相聚集长大越明显(图 6c 和图 7c). 这与锻造温度较低, 遗存的 α_2 相成为晶核, 在热暴露过程中元素扩散, 导致其长大所致.

3 结 论

(1) 经温度 1 025 °C 锻造的 $\text{Ti}_2\text{AlNb}/\text{TC11}$ 双合金接头显微组织在 50 h 热暴露期间即有 $\text{B}_2 \rightarrow \beta + \text{O}$ 分解发生, 使 β 相数量增加, 其形状为条形和球形, 随热暴露延长至 100 h β 相有所粗化, 体积分数

有所增加.

(2) 995 °C 热暴露时, 在接头和 Ti_2AlNb 基体侧中的 α_2 相发生向 B_2 晶界迁移, 随热暴露时间延长, α_2 在 B_2 晶界偏聚成块, 接头位置 α_2 相偏聚不明显是因为此处铝、铌含量低于 Ti_2AlNb 基体.

(3) 在热暴露过程期间, O 相粗化是由于原始 O 相叠加了 B_2 相分解而来的次生 O 相所致.

参考文献:

- [1] 刘莹莹, 姚泽坤, 郭鸿镇. 航空发动机用双性能盘的制造技术研究进展[J]. 材料导报, 2007, 12(21): 95-99.

- Liu Yingying, Yao Zekun, Guo Hongzhen. Research advances in manufacture technique of dual property disk applied to aircraft engine [J]. Mater Rev, 2007, 12(21): 95–99.
- [2] Chen C C. Process development for dual property titanium disk [J]. Experiment Verification of Process Models, USA, 1983: 94–98.
- [3] James 'C Williams. Materials requirements for aircraft engines [A]. Aerospace thermal structures and materials for a new Era [C]// Edited by Eral A Thornton, AIAA, 1995: 360–372.
- [4] 阿列克山大 J D. 宇航材料的锻造和性能 [M]. 贺开运, 译. 北京: 国防工业出版社, 1985.
- [5] 张永刚, 韩雅芳, 陈国良. 金属间化合物结构材料 [M]. 北京: 国防工业出版社, 2001.
- [6] 波诺马廖夫 B A. 航空发动机的现状与未来 [M]. 姚学敏, 朱会生, 译. 北京: 国防工业出版社, 1987.
- [7] 姚泽坤, 张梅林, 梁新民, 等. 热力耦合作用对 TAC-4B 和 TC11 合金焊接界面硬度和显微组织的影响 [J]. 焊接学报, 2004, 25(2): 125–128.
- Yao Zekun, Zhang Meilin, Liang Xinmin, *et al.* Influence of heat force coupling acting on micro-hardness and microstructures at welds seam of TAC-4B/TC11 alloy [J]. Transactions of the China Welding Institution, 2004, 25(2): 125–128.
- [8] 左从进, 李晋炜, 余 伟, 等. 高温钛合金 Ti-55 与 Ti-60 电子束焊接接头性能 [J]. 焊接学报, 2011, 32(4): 103–106.
- Zuo Congjin, Li Jinwei, Yu Wei, *et al.* Tensile performance of Ti-55 and Ti-60 joints welded by electron beam welding [J]. Transactions of the China Welding Institution, 2011, 32(4): 103–106.
- [9] 秦 春, 姚泽坤, 周 伟, 等. 热暴露对 Ti-24Al-15Nb-1.5Mo/TC11 焊接界面显微硬度和元素分布的影响 [J]. 焊接学报, 2012, 33(8): 33–36.
- Qin Chun, Yao Zekun, Zhou Wei, *et al.* Effect of thermal exposure on microhardness and element distribution in welding interface [J]. Transactions of the China Welding Institution, 2012, 33(8): 33–436.
- [10] Tan L J, Yao Z K, Qin C, *et al.* Linear friction and electron beam welded joints of $\text{Ti}_2\text{AlNb}-\text{C11}$ [J]. Advanced Materials Research, 2010, 97/101: 3895–3898.

作者简介: 贾 倩, 女, 1988 年出生, 硕士研究生. 主要从事钛合金的双合金方面的研究. Email: beixi19880610@163.com

通讯作者: 姚泽坤, 男, 博士研究生导师. Email: yzekun@nwu.edu.cn

Metal and Electronic Material , General Research Institute for Nonferrous Metals , Beijing 100088 , China) . pp 75 – 78

Abstract: The optical microscope , scanning electron microscope (SEM) and electron back scattered diffraction (EBSD) were used to analyze the microstructure in different regions of refill friction spot welded (RFSW) joints. The results showed that complete dynamic recrystallization occurred in the nugget zone with fine equiaxial grains , and much finer grains existed at the bottom. The nugget zone had no obvious texture. Part dynamic recrystallization occurred in the TMAZ which contained fine equiaxial grains and partly recovery grains with deformed structure. An obvious interface existed between the nugget zone and TMAZ , and its grain was much finer than those on both sides , and the grain boundary was denser.

Key words: refill friction spot welding; aluminium-lithium alloy; microstructure evolution; electron back scattered diffraction

Microstructure evolution after thermal exposure in weld interface of $Ti_2AlNb/TC11$ dual alloy forged at different temperatures

JIA Qian^{1,2} , YAO Zekun^{1,2} , ZHANG Dongya^{1,2} , QIN Chun^{1,2} , TU Weijian^{1,2} , YANG Guobao^{1,2} , GENG Jingdong³ (1. College of Materials Science and Engineering , Northwestern Polytechnical University , Xi'an 710072 , China; 2. ERC of Forging Technique for Less Deformable Materials , Xi'an 710072 , China; 3. Blade Factory of Guizhou Aero-Power Company , Pingba 561114 , China) . pp 79 – 83

Abstract: The microstructure evolution in $Ti_2AlNb/TC11$ dual alloys after near thermal forging , gradient heat treatment and thermal exposure at 550 °C for 50 h and 100 h , respectively , was investigated with optical microscope (OM) and transmission electron microscope (TEM) . The results show that $B2 \rightarrow O + \beta$ decomposition occurred in the welded seam and Ti_2AlNb matrix , and α_2 phase migrated to the grain boundary of B2 during thermal exposure. The time for thermal exposure was longer , the segregation of α_2 phase at grain boundary was severer. And α_2 phase agglomerated into block when the thermal exposure time was 100 h. Also , the β phase grew coarse and its volume percentage increased simultaneously. If Al and Nb contents were large in the joint , α_2 phase would agglomerate at grain boundary , the original O phase overprinting with the secondary O phase decomposed from B2 phase would coarsen.

Key words: dual alloys; near thermal forging; thermal exposure; microstructure

Influence of weld strength match on distribution of stress triaxiality for aluminum alloy welded joint

ZHU Hao^{1,2} , GUO Zhu^{1,2} , CUI Shaopeng^{1,2} , WANG Yanhong^{1,2} (1. Hebei Provincial Key Laboratory of Traffic Engineering materials , Shijiazhuang TieDao University , Shijiazhuang 050043 , China; 2. School of Materials Science and Engineering , Shijiazhuang TieDao University , Shijiazhuang 050043 , China) . pp 84 – 88

Abstract: The tensile simulation was carried out on 6063 aluminum alloy welded joint with different weld strength matches with software ABAQUS , and the influence of weld strength match

on the distribution of stress triaxiality in aluminum alloy welded joint was studied. At the same time , the influence of HAZ width on the distribution of stress triaxiality in welded joint was studied in each strength match condition. The results indicate that the stress state in welded joints with different weld strength matches was complicated , compared to the base material. Bounce in the stress triaxiality existed in the boundary between the base material and HAZ and between the weld and HAZ. The maximum of stress triaxiality in high strength match welded joint was the largest. On the contrary , the maximum of stress triaxiality in low strength match welded joint was the least. Under the condition of equal strength match , the position of the maximal stress triaxiality changed from the boundary between the base material and HAZ to the boundary between the weld and HAZ with the increasing of the width of HAZ. Under the condition of high strength match , the maximum of stress triaxiality appeared in the boundary between the weld and HAZ , and the maximum of stress triaxiality reduced gradually with the increasing of the width of HAZ. However , under the condition of low strength match , the maximum of stress triaxiality appeared in the boundary between the base material and HAZ , and the maximum of stress triaxiality also reduced gradually with the increasing of the width of HAZ.

Key words: aluminum alloy welded joint; strength match; HAZ; stress triaxiality; FEA

A control technique for electron-beam scan welding

WEI Shouqi , LI Xuejiao , MO Jinhai (College of Mechanical & Electrical Engineering , Guilin University of Electronic Technology , Guilin 541004 , China) . pp 89 – 92 , 96

Abstract: In electron-beam (EB) scan welding , the 2D seam tracking could be approximated by combination of limited line segments and basic arc graphics , hence the whole welding processes could be divided into 3 steps: tracing of teaching , calculating of tracking data , and scan welding. In these processes , three main problems , non-vertical of $x-y$ scanning axis , distortion of scanning track and defocusing of EB spot could be solved by proper conversion of oblique and rectangular coordinates , dynamic correction of deflection scanning magnetizing current with EB's deflection amplitude and velocity , and dynamic correction of focusing magnetizing current with EB's deflection vector , respectively. The welding results with "track & field" type seam tracking reveal that , eccentric distance is above 0.08 mm , depth error is lower than 0.13 mm , width error in surface is lower than 0.16 mm. The proposed welding method could precisely repeat the seam tracking and obtain excellent welding quality.

Key words: electron-beam scan welding; coordinate conversion; scanning track distortion; electron-beam spot defocusing

Test and analysis on corrosion resistance of MWEDM surfaces

ZHANG Bin^{1,2} , GUO Libin¹ , CUI Hai^{1,3} , ZHANG Huigang¹ (1. College of Mechanical and Electrical Engineering , Harbin Engineering University , Harbin 150001 , China; 2. Library , Harbin Engineering University , Harbin 150001 , China; 3. Engineering Training Center , Harbin Engineering University , Harbin 150001 , China) . pp 93 – 96